Sulfate was a trace constituent of Archean seawater

Sean A. Crowe *et al.*

Science **346**, 735 (2014);
DOI: 10.1126/science.1258966

absorption spectra (*23*), 15 ± 2 (statistical) ± 3 (systematic) nW m^{-2} sr^{-1} at 1.4 μm, is independently consistent with the sum of the IHL and IGL backgrounds, within the uncertainties in all measurements.

An EOR interpretation of these measurements would result in a large background, as the contrast factor is larger than that of IHL, 10 to 100 for EOR models (*3*, *6*). The implied EOR background (see Table 1) originating from high redshifts is difficult to justify due to the overproduction of metals and x-ray background photons (*24*).

Our results indicate that a substantial fraction of the EBL at optical and near-infrared wavelengths originates from stars outside of galaxies (with boundaries as traditionally defined). This in turn adds to the cosmic energy budget and, depending on the mass characteristics and spectrum of the population responsible, could help alleviate the "photon underproduction crisis" (*25*) and the "missing baryon problem" (*26*). We see no evidence for a detected EOR background component in our data. Multiwavelength fluctuation measurements extending into the optical will help discriminate the EOR background component using the redshifted Lyman cutoff, and future spectroscopic measurements will enable tomographic measurements to determine the history of IHL production.

REFERENCES AND NOTES

1. A. Cooray, J. J. Bock, B. Keatin, A. E. Lange, T. Matsumoto, *Astrophys. J.* **606**, 611–624 (2004).
2. A. Kashlinsky, R. Arendt, J. P. Gardner, J. C. Mather, S. H. Moseley, *Astrophys. J.* **608**, 1–9 (2004).
3. E. R. Fernandez, E. Komatsu, I. T. Iliev, P. R. Shapiro, *Astrophys. J.* **710**, 1089–1110 (2010).
4. B. Yue, A. Ferrara, R. Salvaterra, Y. Xu, X. Chen, *Mon. Not. R. Astron. Soc.* **433**, 1556–1566 (2013).
5. A. Cooray, Y. Gong, J. Smidt, M. G. Santos, *Astrophys. J.* **756**, 92 (2012).
6. A. Cooray *et al.*, *Nature* **490**, 514–516 (2012).
7. A. Kashlinsky, R. G. Arendt, J. Mather, S. H. Moseley, *Nature* **438**, 45–50 (2005).
8. A. Kashlinsky, R. G. Arendt, J. Mather, S. H. Moseley, *Astrophys. J.* **654**, L5–L8 (2007).
9. A. Kashlinsky *et al.*, *Astrophys. J.* **753**, 63 (2012).
10. R. I. Thompson, D. Eisenstein, X. Fan, M. Rieke, R. C. Kennicutt, *Astrophys. J.* **666**, 658–662 (2007).
11. T. Matsumoto *et al.*, *Astrophys. J.* **742**, 124 (2011).
12. N. Cappelluti *et al.*, *Astrophys. J.* **769**, 68 (2013).
13. M. Zemcov *et al.*, *Astrophys. J. Suppl. Ser.* **207**, 31 (2013).
14. J. Bock *et al.*, *Astrophys. J. Suppl. Ser.* **207**, 32 (2013).
15. M. F. Skrutskie *et al.*, *Astron. J.* **131**, 1163–1183 (2006).
16. K. Helgason, M. Ricotti, A. Kashlinsky, *Astrophys. J.* **752**, 113 (2012).
17. K. Tsumura *et al.*, *Publ. Astron. Soc. Japan* **65**, 119 (2013).
18. J. Pyo, T. Matsumoto, W.-S. Jeong, S. Matsuura, *Astrophys. J.* **760**, 102 (2012).
19. T. D. Brandt, B. T. Draine, *Astrophys. J.* **744**, 129 (2012).
20. A. Lawrence *et al.*, *Mon. Not. R. Astron. Soc.* **379**, 1599–1617 (2007).
21. E. R. Fernandez, E. Komatsu, *Astrophys. J.* **646**, 703–718 (2006).
22. L. R. Levenson, E. L. Wright, B. D. Johnson, *Astrophys. J.* **666**, 34–44 (2007).
23. H.E.S.S. Collaboration., *Astron. Astrophys.* **550**, A4 (2013).
24. P. Madau, J. Silk, *Mon. Not. R. Astron. Soc.* **359**, L37–L41 (2005).
25. J. A. Kollmeier *et al.*, *Astrophys. J.* **789**, L32 (2014).
26. M. Fukugita, C. J. Hogan, P. J. E. Peebles, *Astrophys. J.* **503**, 518–530 (1998).
27. K. Tsumura *et al.*, *Proc. Astron. Soc. Japan* **65**, 120 (2003).
28. A. Franceschini, G. Rodighiero, M. Vaccari, *Astron. Astrophys.* **487**, 837–852 (2008).

ACKNOWLEDGMENTS

Our thanks to O. Doré, J. Filippini, and K. Ganga for useful conversations and comments throughout the course of this work and K. Helgason for kindly providing models of the statistics of the near-infrared CIB. The authors acknowledge the excellent support from the NASA sounding rockets program that was essential in developing, testing, qualifying, launching, and recovering our payloads. The CIBER auto- and cross-power spectra are available for public download at http://ciber.caltech.edu/zemcovetal. This work was supported by NASA APRA research grants NNX07AI54G, NNG05WC18G, NNX07AG43G, NNX07AJ24G, and NNX10AE12G. Initial support was provided by an award to J.B. from the Jet Propulsion Laboratory's Director's Research and Development Fund. Japanese participation in CIBER was supported by KAKENHI (20·34, 18204018, 19540250, 21340047, and 21111004) from Japan Society for the Promotion of Science (JSPS) and the Ministry of Education, Culture, Sports, Science and Technology (MEXT). Korean participation in CIBER was supported by the Pioneer Project from Korea Astronomy and Space Science Institute (KASI). M.Z. and P.K. acknowledge support from NASA Postdoctoral Program fellowships, A.C. acknowledges support from an NSF CAREER award AST-0645427 and NSF AST-1313319, and K.T. acknowledges support from the JSPS Research Fellowship for Young Scientists. This publication makes use of data products from the Two Micron All Sky Survey (2MASS), which is a joint project of the University of Massachusetts and the Infrared Processing and Analysis Center/California Institute of Technology, funded by the National Aeronautics and Space Administration and the National Science Foundation. This work made use of images and/or data products provided by the National Optical Astronomy Observatory (NOAO) Deep Wide-Field Survey (NDWFS), which is supported by NOAO, operated by AURA, Inc., under a cooperative agreement with the National Science Foundation.

SUPPLEMENTARY MATERIALS

www.sciencemag.org/content/346/6210/732/suppl/DC1
Materials and Methods
Supplementary Text
Figs. S1 to S27
Tables S1 to S2
References (*29*–*55*)

1 July 2014; accepted 3 October 2014
10.1126/science.1258168

EARLY EARTH

Sulfate was a trace constituent of Archean seawater

Sean A. Crowe,[1,2]*† Guillaume Paris,[3]* Sergei Katsev,[4] CarriAyne Jones,[1,2] Sang-Tae Kim,[5] Aubrey L. Zerkle,[6] Sulung Nomosatryo,[7] David A. Fowle,[8] Jess F. Adkins,[3] Alex L. Sessions,[3] James Farquhar,[9] Donald E. Canfield[2]

In the low-oxygen Archean world (>2400 million years ago), seawater sulfate concentrations were much lower than today, yet open questions frustrate the translation of modern measurements of sulfur isotope fractionations into estimates of Archean seawater sulfate concentrations. In the water column of Lake Matano, Indonesia, a low-sulfate analog for the Archean ocean, we find large (>20 per mil) sulfur isotope fractionations between sulfate and sulfide, but the underlying sediment sulfides preserve a muted range of $\delta^{34}S$ values. Using models informed by sulfur cycling in Lake Matano, we infer Archean seawater sulfate concentrations of less than 2.5 micromolar. At these low concentrations, marine sulfate residence times were likely 10^3 to 10^4 years, and sulfate scarcity would have shaped early global biogeochemical cycles, possibly restricting biological productivity in Archean oceans.

Sulfur interacts with carbon and oxygen in global biogeochemical cycles that regulate Earth's surface chemistry and biology (*1*). At 28 mM, sulfate is abundant in modern seawater, fueling extensive sedimentary microbial sulfate reduction (MSR) (*2*). At these concentrations, MSR typically imparts large sulfur isotope fractionations (*3*), allowing the use of sulfur isotopes to reconstruct past global change (*4*, *5*). Small sulfur isotope fractionations preserved in bulk pyrite from Archean (>2400 million years ago) rocks led to the original conclusion that the Archean oceans contained <200 μM sulfate, or ~1% of modern seawater (*5*). The distribution of mass-independent sulfur isotopes in Archean sediments (*4*, *6*–*8*) and box models of global sulfur cycling (*9*) imply even lower Archean seawater sulfate of <60 to 80 μM. Paradoxically, microscale sulfur isotope data from Archean pyrites (*10*–*12*) reveal large sulfur isotope fractionations of up to 40 per mil (‰) in the Archean—fractionations only seen at hundreds to thousands of micromolar sulfate in modern environments (*13*–*15*). Electron-donor availability (*3*, *16*) and MSR rate (*3*, *16*, *17*), however, also exert influence, with larger fractionation typically imparted when electron donors limit sulfate-reduction rates, allowing the

[1]Department of Microbiology and Immunology and Department of Earth, Ocean, and Atmospheric Sciences, University of British Columbia, Vancouver, British Columbia, Canada. [2]NordCEE and Department of Biology, University of Southern Denmark, Odense, Denmark. [3]Department of Geological and Planetary Sciences, California Institute of Technology, Pasadena, CA 91125, USA. [4]Large Lakes Observatory and Department of Physics, University of Minnesota, Minneapolis, MN 55812, USA. [5]School of Geography and Earth Sciences, McMaster University, Hamilton, Ontario, Canada. [6]Department of Earth and Environmental Sciences, University of St. Andrews, St. Andrews, UK. [7]Research Center for Limnology, Indonesian Institute of Sciences, Cibinong, West Java, Indonesia. [8]Department of Geology, University of Kansas, Lawrence, KS 66045, USA. [9]Department of Geology, University of Maryland, College Park, MD 20742, USA.
*These authors contributed equally to this work. †Corresponding author. E-mail: sacrowe1@gmail.com

unexplored possibility for large fractionations in low-sulfate (<100 μM) environments.

We explored sulfur isotope fractionation in Lake Matano, Indonesia, an extremely low-sulfate analog for the Archean oceans (*18*). Lake Matano is a persistently stratified ferruginous (Fe^{2+}-rich) lake, where dissolved ferrous iron (Fe^{2+}) accumulates below a chemocline located at ~115 m depth (Fig. 1A). The upper waters of Lake Matano have sulfate concentrations of less than 30 μM (Fig. 1B), far lower than that of the natural environments studied for sulfur isotope fractionation thus far (*13*, *14*) and lower than previous upper limits for Archean seawater (*5*, *8*, *9*). MSR is active within Lake Matano's water column, and peak rates of 30 to 40 nM day^{-1} are reached at sulfate concentrations of between 5 and 10 μM (*11*) (Fig. 1C).

We measured the $\delta^{34}S$ values of sulfate and sulfide in Lake Matano's water column (Fig. 1D) and in the underlying sediments (*19*, *20*). The $\delta^{34}S$ values of sulfate ranged from 8.1‰ within the surface waters to 39.1‰ in the lower reaches of the chemocline, where sulfate is present at barely detectable concentrations (Fig. 1D). Sulfate reduction in the chemocline thus leads to strong isotopic fractionation, despite extremely low sulfate concentrations, favoring the incorporation of ^{32}S into the sulfide produced. Measurements of water-column sulfides reveal $\delta^{34}S$ values from −13.2 to 5.4‰ (table S1), demonstrating that they record large fractionations with a range in $\delta^{34}S$ of up to 18.6‰. Depending on the depths considered, the $\delta^{34}S$ value of water-column sulfides translates to an appreciable isotopic difference ($\Delta^{34}S_{SO_4-H_2S}$) between water-column sulfide and the surface-water sulfate pool of up to 23‰.

We used both a Rayleigh distillation model and a one-dimensional (1D) reaction-diffusion model to calculate sulfur isotope fractionation factors. Rayleigh models underestimate fractionation in open systems (*21*, *22*) like Lake Matano and therefore provide minimum estimates of the true fractionation. Using the Rayleigh model, we obtain a fractionation factor ($\varepsilon_{SO_4-H_2S}$) of 21 ± 1‰ (*16*) (Fig. 2A). To further assess the true magnitude of fractionation during MSR, we constructed an open-system, reaction-diffusion model. As expected, applying the fractionation factor obtained from the Rayleigh model to the reaction-diffusion model underestimates the fractionation observed (Fig. 2B), whereas fractionations ranging between 20 and 70‰ encompass our entire sulfur isotope data set (Fig. 2B). The best fit with constant fractionation, independent of sulfate concentrations, comes from a fractionation factor of 35‰. As MSR proceeds, sulfate concentrations decrease (Fig. 1B), probably shifting MSR from organic matter limitation, which allows expression of large isotope fractionation, to sulfate limitation, which progressively mutes fractionation as sulfate concentrations decrease (*3*, *16*). We therefore also tested a model with fractionation of 70‰ at sulfate concentrations of >6 μM, with a linear decrease to 0‰ when sulfate is exhausted, obtaining an equally good fit. Regardless of the model used, these trends in the $\delta^{34}S$ values of sulfate illustrate large isotope fractionations down to sulfate concentrations below 6 μM (Fig. 2, A and B), confirming that MSR can produce large isotope fractionations at sulfate concentrations more than one order of magnitude lower than previously demonstrated (*5*, *14*, *15*).

Sediments under the chemocline record the integrated $\delta^{34}S$ values of sulfide exported from the water column and exhibit a range of $\delta^{34}S$ values from −4.2 to 6.6‰, with a mean of 2.5 ± 2.5‰ (Fig. 2C). These isotopic compositions are consistent with the range of $\delta^{34}S$ values observed in the water column and predicted by our fractionation models (Fig. 2, A and B) and are up to 14.9‰ lower than that of sulfate in the surface waters of the lake (table S1). Reaction-diffusion models with either a constant fractionation of 35‰ or a variable fractionation of 70‰ that decreases below 6 μM sulfate yield integrated sulfide export with $\delta^{34}S$ values of 3.8 and 2.7‰ (Fig. 2C), respectively. These $\delta^{34}S$ values are similar to the mean of measured sediment sulfides, in contrast to the model with a 20‰ fractionation, which yields a sulfide export flux at the far maximum range of the sediment $\delta^{34}S$ values (6.5‰) and outside of the standard deviation of the sediment mean.

The lack of a full expression of water-column sulfur isotope fractionation in bulk $\delta^{34}S$ measurements of sedimentary sulfides is due to the depletion of sulfate to low concentrations in the chemocline and the development of a strong water-column gradient in sulfate concentration and isotopic composition. As a result, $\delta^{34}S$ values of sulfate increase with decreasing sulfate concentrations (Fig. 1, B and C), leading to a reservoir effect and the production of correspondingly ^{34}S-enriched sulfide, despite the strong fractionation imparted during sulfate reduction. In the

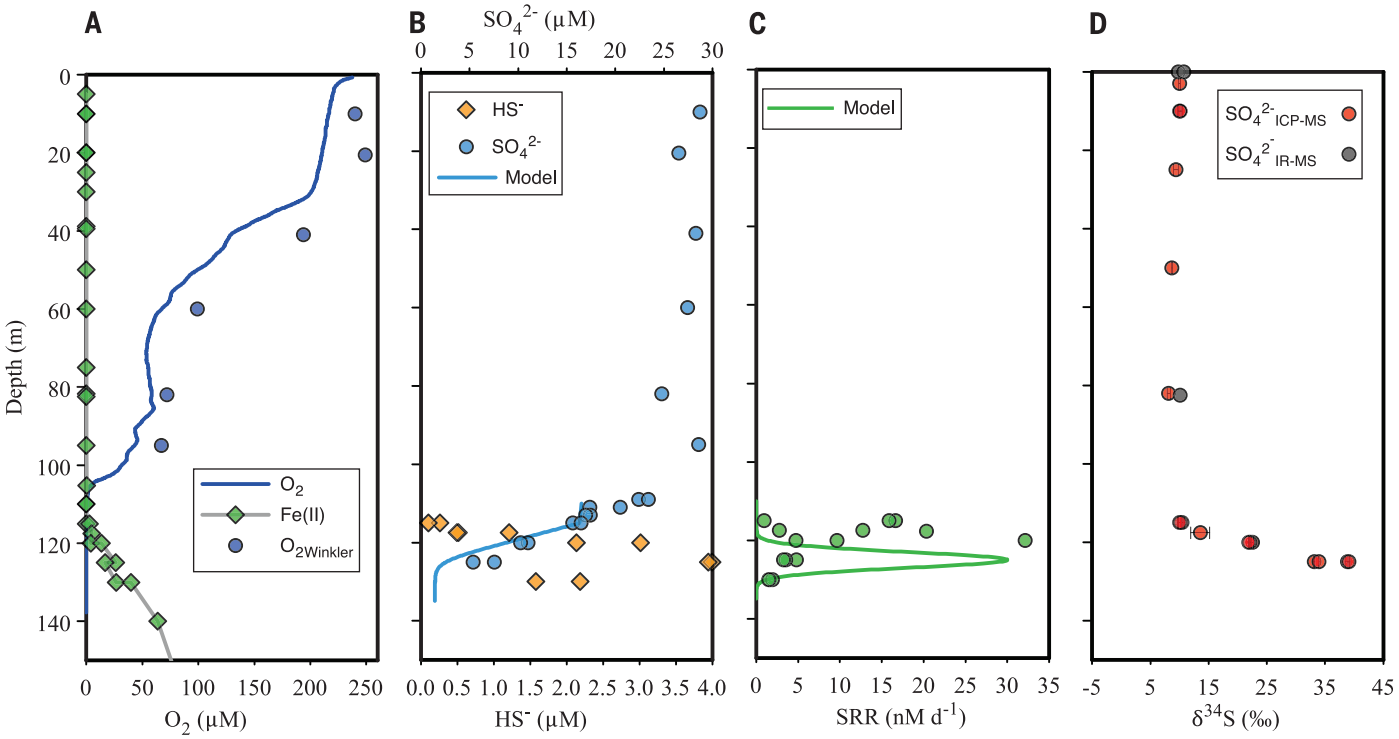

Fig. 1. Vertical chemical profiles in Lake Matano. (**A**) Dissolved O_2 and Fe^{2+}. (**B**) SO_4^{2-} and HS^- (solid line shows modeled SO_4^{2-} concentrations). (**C**) Sulfate-reduction rates (SRRs) (solid line depicts SRRs imposed in the 1D reaction-transport model). d, day. (**D**) $\delta^{34}S$ value of SO_4^{2-}. ICP-MS, inductively coupled plasma mass spectrometry; IR-MS, isotope-ratio mass spectrometry. Data in (A) to (C) come from (*32*), except model results.

end, the net isotopic fractionation between lake-surface sulfate and sedimentary sulfide is only ~7.5‰. A similar effect has been observed in other lakes, albeit at much higher sulfate concentrations (*14*, *15*).

Compilations of the S-isotope composition of Archean sulfides from bulk sediment analyses suggest that the expression of S-isotope fractionation in the Archean was typically less than ~10‰ (Fig. 3). Though most Archean sulfides display little fractionation at the scale of bulk sediment analyses, up to 30‰ (Fig. 3) variability can be observed in the $\delta^{34}S$ of some Archean bulk sediment analyses. Microscale analyses also reveal a broader range in $\delta^{34}S$ of more than 40‰, implying that much larger isotope fractionations were possible (*10*–*12*). The scatter of sulfur isotope data around the Archean MIF-S array (*23*) supports the idea that microbial sulfate reduction in the Archean was accompanied by large sulfur isotope fractionations, possibly more than 40‰, but that the expression of this isotope fractionation at the scale of bulk sedimentary sulfides was muted, similar to our observations in Lake Matano.

To test possible upper limits on Archean seawater sulfate concentrations, we have adapted our reaction-diffusion model to simulate a stratified Archean ocean water column. Like in Lake Matano, we expect that pelagic MSR would have ensued under the ferruginous ocean conditions dominating marine chemistry throughout much of the Archean eon (*24*). In an approach similar to previous models for sedimentary S-isotope fractionation (*5*), we varied seawater sulfate concentrations and computed the integrated $\delta^{34}S$ of sulfide exported from the water column to underlying sediments (Fig. 4). We also assume that MSR would take place in sediments, so we modeled the $\delta^{34}S$ of diagenetic sulfides formed under a range of overlying seawater sulfate concentrations.

Our water-column model shows that at modest MSR rates, comparable to those measured in the Chilean oxygen minimum zone (*25*), appreciable sulfate drawdown occurs with surface seawater sulfate concentrations in the low micromolar range (Fig. 4, A and B). Fractionation factors typical for marine environments (30‰), and justified as a conservative estimate based on microscale measurements of $\delta^{34}S$ in Archean pyrites, translate to a large range in the $\delta^{34}S$ of pelagic sulfate and sulfide (Fig. 4C), showing that reservoir effects similar to those in Lake Matano develop under conditions typical for stratified marine environments. Due to a combination of sulfate drawdown, reservoir effects, and decreased isotope fractionation at low sulfate concentrations, the integrated sulfide exported from the modeled Archean water column has $\delta^{34}S$ values closer to seawater sulfate than would be expected due to the isotope fractionation imparted. The imparted fractionation is best reflected by the sulfide produced in the upper regions of the water column.

Application of a constant fractionation factor of 30‰ in our models results in large differences between the $\delta^{34}S$ values of seawater sulfate and bulk pyrites of 15 to 23‰ (Fig. 4D). Comparing these modeled $\delta^{34}S$ values for sulfide with the distribution of $\delta^{34}S$ in bulk Archean sulfides (yellow diamond distribution plot in Fig. 4D) and assuming seawater $\delta^{34}S$ of 5‰ [the range reported is 3 to 8‰ (*26*–*28*)] shows that these large differences are not supported by the bulk pyrite record. It therefore implies that other processes, such as sulfate limitation of MSR, were at play in the Archean. Conservatively applying a fractionation factor that decreases below 6 μM sulfate, a sulfate concentration that imparts large fractionation in Lake Matano, brings modeled differences between the $\delta^{34}S$ of seawater sulfate and bulk pyrites into a range supported by the Archean bulk pyrite record (Fig. 4D). Under this scenario, both water-column and sediment models predict that MSR would impart bulk sediment sulfide $\delta^{34}S$ values of more than 10‰ lighter than seawater sulfate at sulfate concentrations more than ~5 μM (Fig. 4D). Comparison under this scenario suggests that more than half of the measured sulfide $\delta^{34}S$ values could be described by deposition at seawater sulfate concentrations between 1 and 2.5 μM, and more than 90% deposited at seawater sulfate concentrations <5 μM (Fig. 4D). Taking into consideration that the $\delta^{34}S$ value of seawater sulfate may have reached up to 15‰ in the Neoarchean, and that $\delta^{34}S$ values in pyrite may also include contributions from ^{34}S-enriched photochemical sources (*29*), the concentration window may have extended as high as 10 to 15 μM. Higher seawater sulfate concentrations would have left bulk sulfide $\delta^{34}S$ values much lighter and are therefore not supported by the sedimentary $\delta^{34}S$ sulfide record. The ~30‰ variability observed at the scale of some bulk sediments could be imparted by dynamic processes that cause changes in the concentration of sulfate, the rate of sulfate transport into the sulfate-reduction zone, the rate of MSR (*17*), electron-donor availability (*16*), or the $\delta^{34}S$ of seawater sulfate. These could include variability in depositional depth of sediments analyzed, fluctuations in the depth of mixing, shifting organic matter availability, or variable contributions of atmospheric versus riverine sulfur fluxes to the oceans. Overall, both the limited sulfur isotope fractionation measured at the bulk sediment

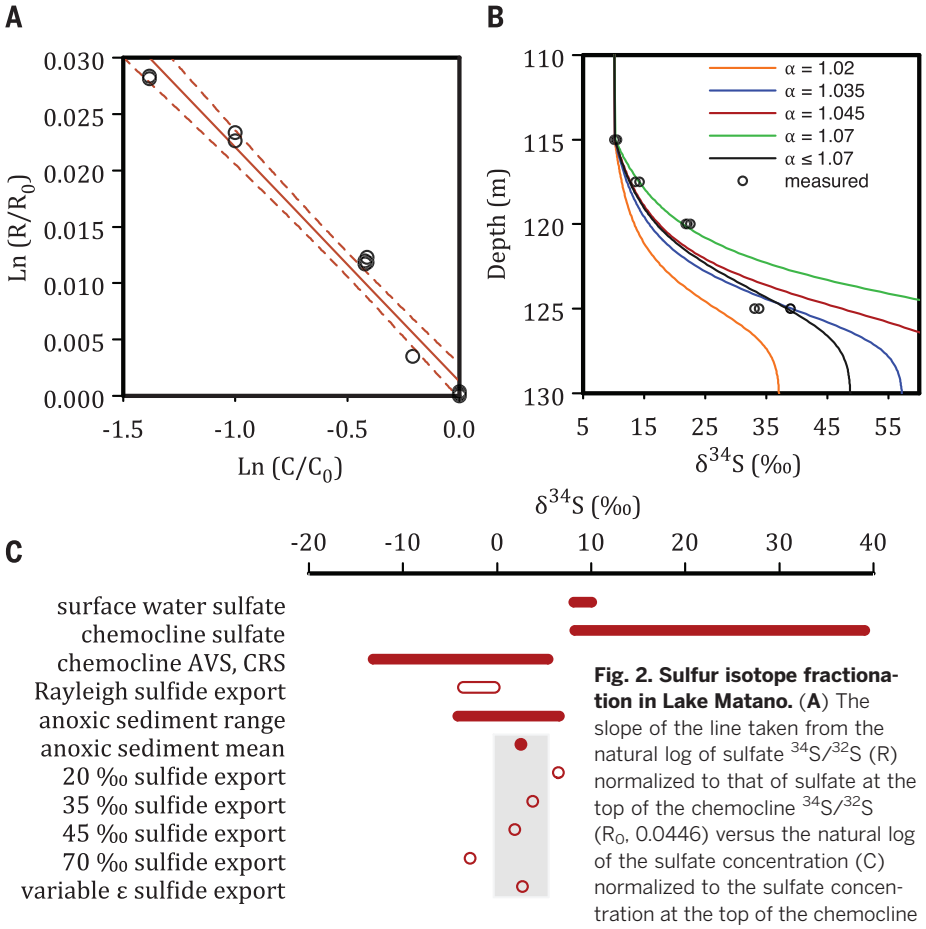

Fig. 2. Sulfur isotope fractionation in Lake Matano. (**A**) The slope of the line taken from the natural log of sulfate $^{34}S/^{32}S$ (R) normalized to that of sulfate at the top of the chemocline $^{34}S/^{32}S$ (R_0, 0.0446) versus the natural log of the sulfate concentration (C) normalized to the sulfate concentration at the top of the chemocline (C_0, 16 μM). The slope of this relation (m = –0.2075) is used to calculate the Rayleigh fractionation factor [$\alpha = (m + 1)^{-1} = 1.0211$]. (**B**) Results from our 1D reaction-diffusion modeling with constant fractionation factors (α) of 1.020, 1.035, 1.045, and 1.070, in addition to a variable fractionation factor with α of 1.070 at sulfate concentrations >6 μM and a linear decrease of α from 1.070 to 1.000 below 6 μM. (**C**) Ranges in $\delta^{34}S$ observed (solid lines and circles) or computed (hollow lines and circles) for different sulfur pools in Lake Matano. The shaded box outlines 1 SD from the anoxic sediment mean. AVS, acid volatile sulfide; CRS, chromium reducible sulfide.

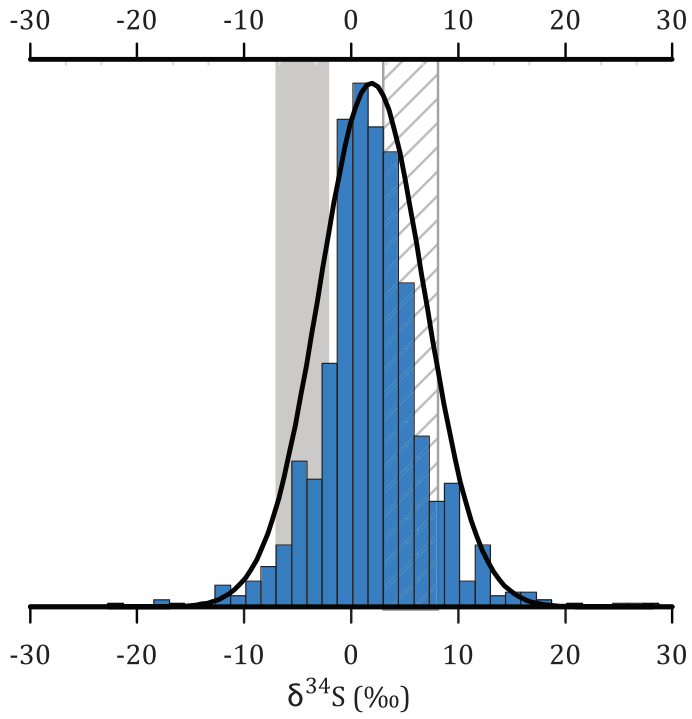

Fig. 3. Compilation of nearly 3000 individual measurements of the $\delta^{34}S$ values of bulk Archean sedimentary sulfides. The black line shows the normal distribution, and the general agreement between the data and the normal distribution suggests a single population. The vertical hatched band delineates the likely range of $\delta^{34}S$ for surface ocean seawater sulfate (*26*–*28*). The vertical gray band shows a 10‰ difference from seawater sulfate. Very few measurements extend beyond this 10‰ difference.

scale and the large isotopic fractionations at the microscale point strongly to sulfate concentrations less than 2.5 μM.

Our results suggest that Archean ocean sulfate concentrations were <0.01% modern seawater, implying very different global sulfur dynamics. With surface seawater sulfate concentrations in the low micromolar range, sulfate residence times (*16*) would have been on the order of 10^3 to 10^4 years, and sulfate could have been poorly mixed in the Archean oceans. Though homogeneity of S isotopes in some Archean barites has been taken as evidence for conservative sulfate behavior (*29*), such conservative behavior at these low seawater sulfate concentrations would imply smaller-than-estimated volcanic and weathering sulfate fluxes to the Archean oceans (*30*). Regardless, the short residence times would have rendered seawater sulfate and its isotopic composition extremely sensitive to perturbations in the global sulfur cycle.

At seawater sulfate concentrations up to 2.5 μM, sediment sulfate reduction would have contributed less than ~10% to sedimentary organic carbon degradation (*16*), leaving the balance to fuel other microbial processes. Organisms also require sulfur as a nutrient, using it for protein synthesis at a typical cellular ratio of 48C:1S:0.45P (*31*); cellular sulfur quotas are thus

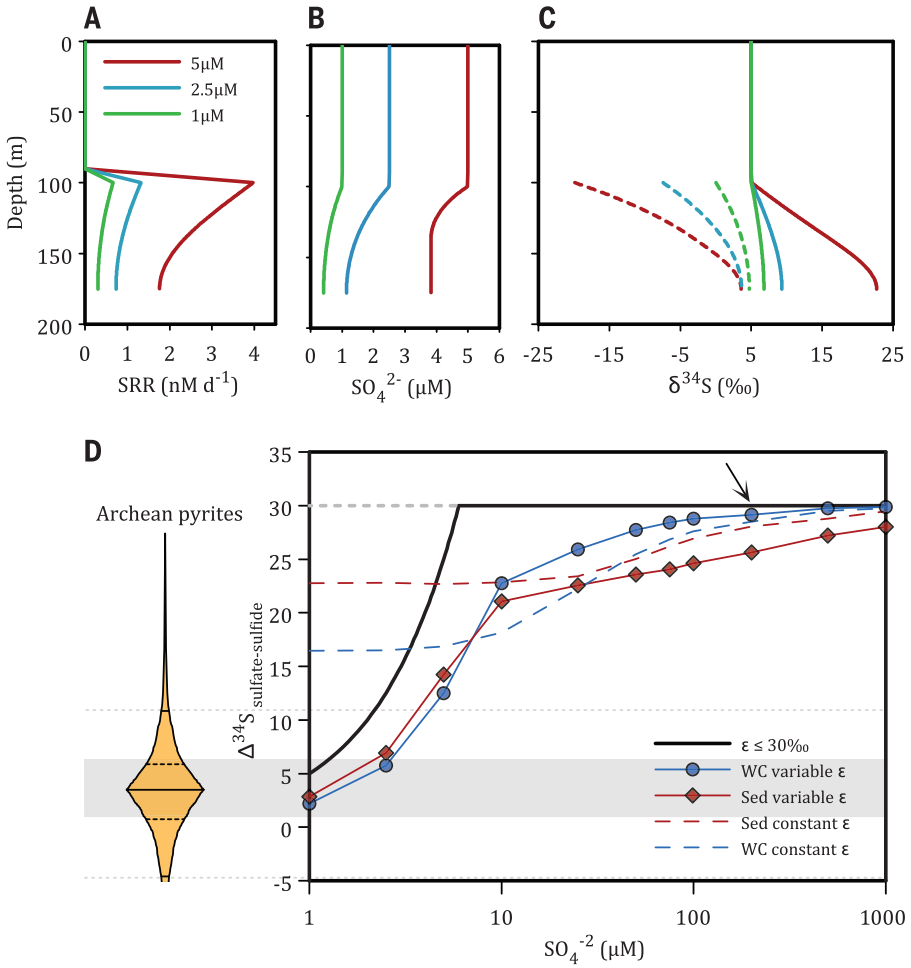

Fig. 4. Models of marine sulfur cycling and isotope fractionation in the Archean eon. (**A**) Modeled rates of microbial sulfate reduction in a stratified Archean ocean water column with different surface seawater sulfate concentrations. (**B**) Resulting sulfate concentration profiles. (**C**) Sulfate (solid lines) and sulfide (dashed lines) $\delta^{34}S$ profiles generated using a variable ε of 30‰ at sulfate concentrations >6 μM that decreases to 0‰ when sulfate is exhausted. (**D**) Mean integrated $\delta^{34}S$ for sulfide produced and exported from the water column to sediments (blue) and diagenetic sulfide (red) at various surface seawater sulfate concentrations. The solid black line indicates the imposed sulfur isotope fractionation factor at different sulfate concentrations (ε ≤ 30‰, justified from microscale analyses of Archean pyrites), and the gray dashed line symbolizes a constant fractionation factor (ε = 30‰). The golden diamond distribution plot at left illustrates sedimentary $\Delta^{34}S_{sulfate\text{-}sulfide}$ calculated from bulk Archean sulfides (from Fig. 3) and using 5‰ as a conservative value for $\delta^{34}S$ of seawater sulfate. The horizontal gray band delineates values between the 25th and 75th percentiles, whereas the horizontal dashed lines delineate the 5th and 95th percentiles, encompassing 90% of the Archean data. The arrow demarcates the previous 200 μM threshold for the full expression of sulfur isotope fractionation (*5*).

higher than those of phosphorus. At low concentrations, nutrients such as phosphorus tend to limit biological production, and by analogy, sulfur may have played a more important role as a biologically scarce nutrient.

REFERENCES AND NOTES

1. S. T. Petsch, R. A. Berner, *Am. J. Sci.* **298**, 246–262 (1998).
2. B. B. Jørgensen, *Nature* **296**, 643–645 (1982).
3. D. E. Canfield, *Geochim. Cosmochim. Acta* **65**, 1117–1124 (2001).
4. R. A. Berner, S. T. Petsch, *Science* **282**, 1426–1427 (1998).
5. K. S. Habicht, M. Gade, B. Thamdrup, P. Berg, D. E. Canfield, *Science* **298**, 2372–2374 (2002).
6. Q. J. Guo *et al.*, *Geology* **37**, 399–402 (2009).
7. I. Halevy, D. T. Johnston, D. P. Schrag, *Science* **329**, 204–207 (2010).
8. J. W. Jamieson, B. A. Wing, J. Farquhar, M. D. Hannington, *Nat. Geosci.* **6**, 61 (2013).
9. I. Halevy, *Proc. Natl. Acad. Sci. U.S.A.* **110**, 17644–17649 (2013).
10. J. Farquhar *et al.*, *Proc. Natl. Acad. Sci. U.S.A.* **110**, 17638–17643 (2013).
11. W. W. Fischer *et al.*, *Proc. Natl. Acad. Sci. U.S.A.* **111**, 5468–5473 (2014).
12. B. S. Kamber, M. J. Whitehouse, *Geobiology* **5**, 5–17 (2007).
13. D. E. Canfield, J. Farquhar, A. L. Zerkle, *Geology* **38**, 415–418 (2010).
14. M. L. Gomes, M. T. Hurtgen, *Geology* **41**, 663–666 (2013).
15. M. Nakagawa *et al.*, *Limnol. Oceanogr.* **57**, 974–988 (2012).
16. M. S. Sim, S. Ono, K. Donovan, S. P. Templer, T. Bosak, *Geochim. Cosmochim. Acta* **75**, 4244–4259 (2011).
17. W. D. Leavitt, I. Halevy, A. S. Bradley, D. T. Johnston, *Proc. Natl. Acad. Sci. U.S.A.* **110**, 11244–11249 (2013).
18. S. A. Crowe *et al.*, *Proc. Natl. Acad. Sci. U.S.A.* **105**, 15938–15943 (2008).
19. Materials and methods are available as supplementary materials on *Science* Online.
20. G. Paris, A. L. Sessions, A. V. Subhas, J. F. Adkins, *Chem. Geol.* **345**, 50–61 (2013).
21. M. B. Goldhaber, I. R. Kaplan, *Mar. Chem.* **9**, 95–143 (1980).
22. B. B. Jorgensen, *Geochim. Cosmochim. Acta* **43**, 363–374 (1979).
23. S. Ono *et al.*, *Earth Planet. Sci. Lett.* **213**, 15–30 (2003).
24. S. W. Poulton, D. E. Canfield, *Elements* **7**, 107–112 (2011).
25. D. E. Canfield *et al.*, *Science* **330**, 1375–1378 (2010).
26. E. M. Cameron, K. Hattori, *Chem. Geol.* **65**, 341 (1987).
27. D. E. Canfield, J. Farquhar, *Proc. Natl. Acad. Sci. U.S.A.* **106**, 8123–8127 (2009).
28. I. B. Lambert, T. H. Donnelly, J. S. R. Dunlop, D. I. Groves, *Nature* **276**, 808–811 (1978).
29. D. L. Roerdink, P. R. D. Mason, J. Farquhar, T. Reimer, *Earth Planet. Sci. Lett.* **331–332**, 177–186 (2012).
30. E. E. Stüeken, D. C. Catling, R. Buick, *Nat. Geosci.* **5**, 722–725 (2012).
31. C. T. A. Chen, C. M. Lin, B. T. Huang, L. F. Chang, *Mar. Chem.* **54**, 179–190 (1996).
32. S. A. Crowe *et al.*, *Geobiology* **12**, 322–339 (2014).

ACKNOWLEDGMENTS

We thank A. Sturm and C. Henny for help with fieldwork. S. Poulton provided sediment $\delta^{34}S$ data. A. Hefford helped compile Archean S-isotope data. Funding to S.A.C. was provided by an Agouron Institute Geobiology Fellowship and a *Natural Sciences and Engineering Research Council* of Canada Postdoctoral Fellowship. Additional funding was provided by the Danish National Research Foundation (grant no. DNRF53) and the European Research Council. All data are available in the supplementary materials.

SUPPLEMENTARY MATERIALS

www.sciencemag.org/content/346/6210/735/suppl/DC1
Materials and Methods
Supplementary Text
Figs. S1 and S2
Tables S1 to S5
References (*33*–*68*)
Data S1

21 July 2014; accepted 10 October 2014
10.1126/science.1258966

EARLY EARTH

Neoarchean carbonate-associated sulfate records positive $\Delta^{33}S$ anomalies

G. Paris,[1]* J. F. Adkins,[1] A. L. Sessions,[1] S. M. Webb,[2] W. W. Fischer[1]

Mass-independent fractionation of sulfur isotopes (reported as $\Delta^{33}S$) recorded in Archean sedimentary rocks helps to constrain the composition of Earth's early atmosphere and the timing of the rise of oxygen ~2.4 billion years ago. Although current hypotheses predict uniformly negative $\Delta^{33}S$ for Archean seawater sulfate, this remains untested through the vast majority of Archean time. We applied x-ray absorption spectroscopy to investigate the low sulfate content of particularly well-preserved Neoarchean carbonates and mass spectrometry to measure their $\Delta^{33}S$ signatures. We report unexpected, large, widespread positive $\Delta^{33}S$ values from stratigraphic sections capturing over 70 million years and diverse depositional environments. Combined with the pyrite record, these results show that sulfate does not carry the expected negative $\Delta^{33}S$ from sulfur mass-independent fractionation in the Neoarchean atmosphere.

The sulfur isotopic composition of Archean [3.8 to 2.4 billion years ago (Ga)] sedimentary rocks provides critical evidence that Earth's atmosphere contained very little, if any, free O_2 before the rise of oxygen ~2.4 Ga (*1*–*6*). Most processes on Earth fractionate sulfur isotopes proportionally to their relative mass differences [$\Delta^{33}S = 0$ (*7*)], yet Archean pyrite (FeS_2) commonly deviates from this relationship, skewed toward positive $\Delta^{33}S$ values (*1*, *8*). This mass-independent fractionation (MIF) pattern is widely attributed to photodissociation of SO_2 by ultraviolet (UV) light allowed by the extremely low levels of O_2 and O_3 in Earth's atmosphere at that time (*1*, *6*). In this scenario, coeval sulfate aerosols ultimately deposited in the ocean as dissolved sulfate carry the complementary negative $\Delta^{33}S$ anomalies required by isotopic mass balance (*1*, *2*, *5*, *8*, *9*). Recent experiments (*10*–*12*) and models of the Archean atmosphere (*2*) show a much wider range of MIF patterns, including positive $\Delta^{33}S$ anomalies in sulfate instead of lower-valent S species. Sulfate minerals that would provide a test of the distribution of MIF signal are absent from Archean evaporite sequences—bedded sulfate deposits occur only after the rise of oxygen (*13*). Paleoarchean barites (3.5 to 3.2 Ga) are a notable exception. They carry small, negative $\Delta^{33}S$ values [0 to –1.5‰ (*1*, *14*–*16*)] but have an enigmatic petrogenesis (*17*). No such sulfate record exists for the billion-year interval from Mesoarchean time through the Paleoproterozoic rise of oxygen. Consequently, the notion of an Archean marine sulfate pool with negative $\Delta^{33}S$ values remains largely untested.

Sulfate minerals are not the only portal into the past marine sulfate pool. Small quantities of carbonate-associated sulfate (CAS) have become an important archive for studying marine sulfate in younger successions (*18*). However, the very low sulfate concentrations of Archean carbonates have kept this archive largely out of reach for conventional analytical methods. Two studies measuring Archean CAS suggested that Archean sulfate carried positive $\Delta^{33}S$ (*4*, *19*). However, both studies used large sample sizes (>100 g of $CaCO_3$), raising the risks of lower preservation as well as contamination by pyrite. We recently developed a technique using inductively coupled plasma mass spectrometry to measure both $\Delta^{33}S$ and $\delta^{34}S$ using a few tens of milligrams of low-CAS carbonate (*20*). Greater sensitivity allows the measurement of sulfur isotopes from specific petrographic and sedimentary fabrics with different diagenetic histories, coupled with light and electron microscopy (Fig. 1 and fig. S4), to directly assess sample quality based on the presence of additional S-bearing phases (e.g., organic sulfur, pyrite). In parallel, we applied synchrotron x-ray absorption spectroscopy (XAS) to measure sulfur speciation in these samples. We examined three sedimentary sections from a range of marine paleoenvironments across the Neoarchean Campbellrand carbonate platform (*21*). Section W1 (aragonite sea-floor fans, precipitated laminae, preserved as early diagenetic fabric-retentive dolomite) captures shallow subtidal environments, whereas sections GKP01 and W2 [herringbone, an early marine calcitic cement (*22*), microbial laminae, dolomite, and calcite spar] capture deep subtidal and slope environments (*21*).

The CAS data preserve positive $\delta^{34}S$ values and unambiguously positive $\Delta^{33}S$ values and display significant variability, sometimes at very small scales (Fig. 2 and additional data table S1). The carbonate fabrics contain 5 to 70 parts per million (ppm) sulfate—two orders of magnitude lower than typical Phanerozoic carbonates. Because of such low levels, we consider the potential impacts of contamination and/or sulfide oxidation

[1]Division of Geological and Planetary Sciences, California Institute of Technology, Pasadena, CA 91125, USA. [2]Stanford Synchrotron Radiation Lightsource, Menlo Park, CA 94025, USA.
*Corresponding author. E-mail: gparis@caltech.edu